RSC Advances

PAPER

View Article Online
View Journal | View Issue

Cite this: *RSC Adv.*, 2022, **12**, 36046

Selective Pd recovery from acidic leachates by 3-mercaptopropylphosphonic acid grafted TiO_2: does surface coverage correlate to performance?†

Nick Gys, ‡§[ab] Bram Pawlak, [c] Léon Luntadila Lufungula, [d] Kristof Marcoen, [e] Kenny Wyns,[a] Kitty Baert,[e] Thomas Abo Atia,[af] Jeroen Spooren, [a] Peter Adriaensens, [c] Frank Blockhuys, [d] Tom Hauffman,[e] Vera Meynen, [ab] Steven Mullens[a] and Bart Michielsen *[a]

Modification of metal oxides with organophosphonic acids (PAs) provides the ability to control and tailor the surface properties. The metal oxide phosphonic acid bond (M–O–P) is known to be stable under harsh conditions, making PAs a promising candidate for the recovery of metals from complex acidic leachates. The thiol functional group is an excellent regenerable scavenging group for these applications. However, the research on organophosphonic acid grafting with thiol groups is very limited. In this study, four different metal sorbent materials were designed with different thiol surface coverages. An aqueous-based grafting of 3-mercaptopropylphosphonic acid (3MPPA) on mesoporous TiO_2 was employed. Surface grafted thiol groups could be obtained in the range from 0.9 to 1.9 groups per nm^2. The different obtained surface properties were studied and correlated to the Pd adsorption performance. High Pd/S adsorption efficiencies were achieved, indicating the presence of readily available sorption sites. A large difference in their selectivity towards Pd removal from a spend automotive catalyst leachate was observed due to the co-adsorption of Fe on the titania support. The highest surface coverage showed the highest selectivity (K_d: 530 mL g^{-1}) and adsorption capacity (Q_{max}: 0.32 mmol g^{-1}) towards Pd, while strongly reducing the co-adsorption of Fe on remaining TiO_2 sites.

Received 14th November 2022
Accepted 12th December 2022

DOI: 10.1039/d2ra07214a

rsc.li/rsc-advances

1. Introduction

Platinum group metals (PGMs) are known for their distinct physical and chemical properties such as corrosion resistance, high catalytic activity and good electrical conductivity.[1] PGMs act as the active component in materials and are used in a plethora of fields of which catalysts (*i.e.* petrochemical, pharmaceutical and automobile industry) and electronics account for over 90% of the total demand.[2] PGMs are obtained from low grade primary ores with typical concentrations in the range of 0.01 ppm which are mined in only a few regions worldwide (South Africa, Russia, Zambia). Additionally, the natural availability of PGMs is limited. Combined with the rapid succession of industrial developments and emerging

[a]*Sustainable Materials, Flemish Institute for Technological Research (VITO NV), Boeretang 200, Mol 2400, Belgium. E-mail: bart.michielsen@vito.be*

[b]*Laboratory of Adsorption and Catalysis (LADCA), Department of Chemistry, University of Antwerp, Universiteitsplein 1, Wilrijk 2610, Belgium*

[c]*Analytical and Circular Chemistry (ACC), Institute for Materials Research (IMO), Hasselt University, Agoralaan 1, Diepenbeek 3590, Belgium*

[d]*Structural Chemistry Group, Department of Chemistry, University of Antwerp, Groenenborgerlaan 171, Antwerp 2020, Belgium*

[e]*Research Group Electrochemical and Surface Engineering (SURF), Department Materials and Chemistry, Vrije Universiteit Brussel, Pleinlaan 2, Brussels 1050, Belgium*

[f]*Department of Chemistry, KU Leuven, Celestijnenlaan 200F, Leuven 3000, Belgium*

† Electronic supplementary information (ESI) available: Evolution of the phosphorus concentration during pressure filtration. N_2 physisorption data of the unmodified and 3MPPA modified TiO_2 support with different surface coverages. XRD data of the TiO_2 support. DRIFT spectra of unmodified and 3MPPA modified TiO_2. Negative ToF-SIMS spectra of unmodified and 3MPPA modified TiO_2, with detailed overlay of the S^-, TiO_2SH^- and $C_3H_8PO_3S^-$ ion fragments. DFT calculated adsorption energies and ^{31}P chemical shifts of a selection of different surface conformations of 3MPPA on anatase (101). Impact of the chlorine concentration on the palladium speciation at pH 2 and pH 5. Comparison between non-linear pseudo first-order and non-linear pseudo second-order fitting on the Pd adsorption kinetics. Calculated S···S distances for adjacent 3MPPA groups on anatase (101). XPS S 2p and Pd 3d spectra of 3MPPA modified TiO_2, before and after Pd adsorption. Plot of distribution coefficients and adsorption capacities for metals present in the acidic leachate upon adsorption with unmodified TiO_2 and 3MPPA modified TiO_2 at different surface coverages. Separation factors of Pd relative to Pt, Fe and Cu after adsorption from the acidic leachate for the different surface coverages of 3MPPA. See DOI: https://doi.org/10.1039/d2ra07214a

‡ Current address: Centre for Membrane Separations, Adsorption, Catalysis and Spectroscopy (cMACS), KU Leuven, Celestijnenlaan 200F, 3001 Leuven, Belgium.

§ Current address: Research Group Electrochemical and Surface Engineering (SURF), Vrije Universiteit Brussel, Pleinlaan 2, 1050 Brussels, Belgium.

economies, this creates potential resource scarcities and strong fluctuations in global market prices. Therefore, PGMs are part of the EU list addressing critical raw materials (CRMs), being characterized by a high economic value and a high supply risk.[3]

Thus, to meet the growing demand, the recovery of PGMs from secondary sources such as end-of-life products and spent industrial catalysts is of increasing concern from both economic and environmental point of view.[4,5] Per consequence, the development of recovery technologies is of great interest as this drives the acceleration towards an improved resource efficiency and increasing self-sufficient supply of raw materials. On industrial scale, PGMs are recycled by means of pyrometallurgical processes, followed by hydrometallurgical refining. The latter encompasses leaching under oxidizing, strongly acidic conditions resulting in an aqueous solution of low-concentrated PGMs accompanied with a complex mixture of base metals and anions.[6–8] Several methods exist for the recovery of PGMs from these solutions, such as chemical precipitation, ion exchange, solvent extraction, membrane separation and adsorption.[4,9–11] Among these methods, adsorption is considered an attractive and viable method for the recovery of PGMs due to its high pre-concentration factor, high separation efficiency, ease of operation and relatively low energy consumption and waste generation.[9,10]

Different materials have been investigated as solid sorbents for PGM recovery from aqueous solutions. Surface grafted mesoporous SiO_2 materials (*e.g.* SBA-15, MCM-41) for PGM recovery are by far the best documented in literature,[12] offering high mechanical stability and non-swelling behavior in contrast to polymeric based adsorbents.[13,14] Furthermore, the high surface area and pore volume of these mesoporous silica materials, combined with a tailored and (relatively) narrow pore size are advantageous with regard to adsorption capacity and kinetics. To enhance the affinity and selectivity for PGMs, organic groups containing hetero-elements (N, S) are grafted onto the surface through organosilylation.[9] All these materials show promising PGM adsorption performances, especially sulfur based ligands. Nevertheless, several aspects might hamper their further development. On the one hand, reproducibility issues can arise as organosilanes are sensitive to polymerization in the presence of water[15] depending on the type and number of reactive groups, resulting in multilayer formation and inhomogeneous surface chemistry that can adversely affect the adsorption performance and hydrolytic stability of the organic layer.[16,17] The use of anhydrous organic solvents (*e.g.* toluene) with trace amounts of water is often a prerequisite, especially for organosilanes containing more than one reactive group. On the other hand, leaching of grafted organic groups and the silica backbone becomes prominent under prolonged exposure to harsh conditions (low pH, increased temperature),[18–20] affecting the operational lifetime and applicability in acidic aqueous PGM containing leachates. Ensuring a full monolayer coverage and end-capping of residual surface OH groups increases the stability, but reduces to some extent the tailoring of the surface properties.[15]

To tackle these challenges, research in this field expanding towards organophosphonic acid (PA) grafting of metal oxides (*e.g.* TiO_2, ZrO_2 and Al_2O_3).[21–26] The low susceptibility of PAs towards polymerization makes grafting possible in aqueous solution, enabling sub-monolayer formation with the presence of dangling P=O or P–OH bonds that can potentially influence the adsorption properties. Experimental systematic studies by Roevens *et al.*[27,28] and Tassi *et al.*[29,30] on propylphosphonic acid and phenylphosphonic acid modified TiO_2 show that the modification conditions (concentration, temperature and solvent) and type of PA strongly affect the binding mode (mono-, bi- and tridentate), amount of grafted organic groups and their distribution on the surface. Computational studies revealed complementary insights with regard to the impact of each pristine TiO_2 crystal facet on the binding mode possibilities.[31–35] To extend the functionality and applicability of organophosphonic acid grafted TiO_2, grafting with PAs containing nitrogen or sulfur heteroatoms has gained increasing attention.

The few studies available for grafting with sulfur-based PAs are mainly oriented towards tuning the electronic properties in nanoelectronics devices[36–40] and the development of quantum dot sensitized solar cells.[41–43] Although PGMs have a strong affinity for sulfur functionalities in metal sorption, this research area has remained largely unexplored for organophosphonic acid modified metal oxides. A case study on heavy metal recovery was reported by Mutin *et al.*[44] They reported the synthesis of 12-mercaptododecylphosphonic acid grafted TiO_2 P25 for the adsorption of mercury under alkaline conditions (pH > 9), demonstrating a high hydrolytic stability up to pH 11 with an adsorption capacity of 0.8–0.9 mg g^{-1}. An Trieu *et al.*[45] introduced a S–S functional group onto the surface of ZrO_2 and studied the adsorption properties and reusability for the selective recovery of Pd and Au from acidic (pH = 0.3) industrial electronic wastewater. They compared two modification strategies, *i.e.* a direct grafting using thioctic acid (ZrO_2-TOA) and a two-step grafting process initiated with alendronic acid, in which the phosphonate moieties bind to the surface, followed by an amide coupling with thioctic acid (ZrO_2-AA-TOA). After each adsorption–desorption cycle, the ZrO_2-TOA material exhibited a significant decrease in the adsorption efficiency, eventually reaching only 20% in the 4th cycle. In contrast, the ZrO_2-AA-TOA material maintained a high adsorption and regeneration efficiency up to 80%. These results confirm the higher hydrolytic stability of Zr–O–P bonds compared to Zr–O–C, and highlight promising benefits and prospects in the implementation of organophosphonate grafted metal oxides for PGM recovery under highly acidic conditions (pH < 1). However, the use of complex and bulky ligands *via* a two-step modification protocol can compromise the ease of synthesis and pose challenges in controlling the surface chemistry.

This study focuses on the aqueous-based synthesis of mercaptopropylphosphonic acid (3MPPA) modified mesoporous TiO_2 powder (Hombikat M311) for the selective recovery of Pd from aqueous acidic media. The main goal is to elucidate the correlation between the surface properties, which are altered by using different concentrations of 3MPPA during synthesis, and the metal sorption performance. Hombikat M311 is grafted at different 3MPPA concentrations (20, 50, 100 and 150 mM) followed by Pd adsorption experiments, studying the effect of pH,

kinetics and adsorption capacity. Furthermore, the sorption performance of the synthesized materials is evaluated under relevant conditions *via* Pd sorption from an acidic leachate originating from an automotive exhaust catalyst.

2. Experimental section

2.1 Materials

3-Mercaptopropylphosphonic acid (3MPPA) was purchased from Sikémia. Mesoporous TiO_2 Hombikat M311 (crystal phase: 100% anatase, BET surface of 300 $m^2\ g^{-1}$) was supplied by Sachtleben Chemie GmbH (now VENATOR). $PdCl_2$ (≥99.9%) and solid thiourea was purchased from Sigma Aldrich. HCl (37%, Sigma Aldrich) and NaOH pellets (Sigma Aldrich) were used for pH adjustments. All chemicals were analytic grade reagents and used without further purification.

2.2 Surface modification

4.0 g of Hombikat M311 was added to an aqueous solution of 100 mL 3MPPA and stirred for 24 h under reflux at 90 °C. Modifications were performed with a 3MPPA concentrations of 20, 50, 100 and 150 mM. After modification, the samples were washed by pressure filtration (Sterlitech) to remove unreacted and physisorbed 3MPPA. During this process, the reactant solution was removed, followed by batch pressure filtration with 400 mL H_2O for each washing step. After ten consecutive washing steps (*i.e.* total volume of 4 L), the samples were dried overnight in an oven at 60 °C. The phosphorus concentration in the 10 collected eluates of washing liquid was analyzed by ICP-OES to evaluate the extent of washing (Fig. S.1†). All samples received a systematic name based on the modification conditions, *e.g.* 3MPPA20 represents a sample modified with 20 mM of 3MPPA.

2.3 Instrumentation

Inductively coupled plasma optical emission spectroscopy (Agilent Technologies 5100 ICP-OES) was performed to determine the phosphorus content of the 3MPPA modified samples. Samples were digested in a mixture of 1.5 mL HNO_3 (67–69%), 1.5 mL HF (48%) and 3 mL H_2SO_4 (96%) for 24 hours at 250 °C. After digestion, 16 mL H_3BO_3 (4%) was added to neutralize the HF. The modification degree in number of grafted groups per nm^2 (#groups per nm^2) is calculated from the weight percentage of phosphorus according to eqn (1):

$$\text{mod. degr.}\left(\frac{\#}{\text{nm}^2}\right) = \frac{\text{wt \%(P)} \times N_A}{\text{MM(P)} \times S_{BET} \times 100} \quad (1)$$

in which wt%(P) is the weight percentage of phosphorus in the sample, MM (P) is the molar mass of phosphorus ($g\ mol^{-1}$), S_{BET} ($nm^2\ g^{-1}$) is the surface area of the unmodified TiO_2 powder and N_A is Avogadro's constant (molecules per mol). The experimental error is estimated to be 0.1 groups per nm^2 based on four repeated modifications at fixed synthesis conditions.

Nitrogen sorption measurements were performed at −196 °C on a Quantachrome Quadrasorb SI automated gas adsorption system. Prior to the measurements, unmodified Hombikat was degassed for 16 hours under high vacuum at 200 °C, while a temperature of 60 °C was used for 3MPPA grafted samples. The specific surface area and *C*-constant were calculated using the Brunauer–Emmett–Teller (BET) method and the pore volume and pore size distribution were determined by the Barrett–Joyner–Halenda (BJH) method using the desorption branch. The reader is referred to Fig. S.2 and Table S.1.†

Diffuse reflectance infrared Fourier transform (DRIFT) measurements were performed on a Nicolet 6700 Fourier Transform IR spectrometer (Thermo Scientific), equipped with an electromagnetic source in the mid-IR region (4000–700 cm^{-1}) and a DTGS detector. A resolution of 4 cm^{-1} was used and for each spectrum 100 scans were accumulated. The sample holder contained a 4 wt% diluted sample in KBr and measurements were performed after 30 minutes at room temperature under low vacuum (30 mbar) to reduce the amount of molecular adsorbed water.

X-ray photoelectron spectroscopy (XPS) spectra were collected using a VersaProbe II photoelectron spectroscope (Physical Electronics) with an Al Kα monochromatic X-ray source (1486.71 eV of photons). The vacuum in the analysis chamber was approximately 5×10^{-7} Pa during measurements. High-resolution scans of the Ti 2p, O 1s, C 1s, P 2p, S 2p, Cl 2p and Pd 3d photoelectron peaks were recorded from a spot diameter of 100 μm using a pass energy of 23.4 eV and a step size of 0.1 eV. Measurements were performed with a takeoff angle of 45° with respect to the sample surface. The powders were applied on scotch tape. Data was analyzed with CasaXPS software. Prior to curve fitting, the energy scale of the XPS spectra was calibrated relative to the binding energy of Ti $2p_{3/2}$ (458.5 eV) in $Ti(IV)O_2$.[46] The spin–orbit doublet separation of the S 2p and Pd 3d signals were set to 1.18 eV[47] and 5.30 eV,[48] respectively. Curve fitting was done after a Shirley type background removal, using mixed Gaussian–Lorentzian (50–50%) shapes for S 2p and a Lorentzian function for Pd 3d.

Phosphorus-31 solid-state cross-polarization magic angle spinning (*CP*-MAS) NMR spectra were acquired at ambient temperature on an Agilent VNMRS DirectDrive 400 MHz spectrometer (9.4 T wide bore magnet) equipped with a T3HX 3.2 mm VT probe dedicated for small sample volumes and high decoupling powers. Magic angle spinning (MAS) was performed at 15 kHz using ceramic zirconia rotors of 3.2 mm in diameter (22 μL rotors). The phosphorus chemical shift scale was calibrated to orthophosphoric acid (H_3PO_4) at 0 ppm. Other acquisition parameters used were: a spectral width of 60 kHz, a 90° pulse length of 3.2 μs, a spin-lock field for CP of 80 kHz, a contact time for CP of 0.9 ms, an acquisition time of 15 ms, a recycle delay time of 4 s and 512 accumulations. High power proton dipolar decoupling during the acquisition time was set at 80 kHz. The Hartmann-Hahn condition for CP was calibrated accurately on the samples themselves.

ToF-SIMS measurements were obtained with a TOF.SIMS 5 system from ION-TOF GmbH (Münster, Germany). A 30 keV Bi^{3+} primary ion beam was used in high current bunched mode for high mass resolution (0.70 pA target current, 3 μm lateral resolution). Analysis areas of 100 μm × 100 μm were raster-scanned (128 × 128 pixels) to obtain either positive or

negative secondary ion mass spectra. The primary ion dose was kept below the static limit of 1×10^{13} ions cm^{-2} $analysis^{-1}$. The pressure in the ToF-SIMS main chamber was $\sim 3.5 \times 10^{-8}$ mbar during measurements.

2.4 Quantum chemical calculations

All calculations were performed under Periodic Boundary Conditions (PBC) with the Quantum Espresso (QE) software package[49] using plane waves as basis sets. The Wu & Cohen (WC) modification of the PBE functional[50] was used since it allows for a high-quality description of solid-state materials.[51] Treatment of the core electrons is based on the Projector Augmented Wave (PAW) method.[52] The $1s^2$ electrons are treated as core electrons for C, O and N, whereas the $1s^2 2s^2 2p^6$ electrons are treated as core electrons for Ti and P. An energy cutoff of 60 Ry and a *k*-point grid of $2 \times 2 \times 1$ were used. Dispersion interactions were taken into account by adding an additional term to the DFT total energy based on the DFT-D2 method by Grimme.[53,54] The anatase (101) facet was selected in the model since this is the most exposed facet in the anatase crystal phase of Hombikat M311 titania powder (Fig. S.3 and Table S.2†). A 3-layer slab with a 20 Å vacuum width was constructed using the cif2cell software package[55] and functionalized with 3MPPA. The atoms in the lowest layer of the slab were constrained to their initial bulk positions, while all other atoms were allowed to relax. The adsorption energies (E_{ads}) are calculated as $E_{ads} = E_{(adsorbate+surface)} - (E_{adsorbate} + E_{surface})$, where $E_{(adsorbate+surface)}$ is the energy of the adsorption complex, while $E_{adsorbate}$ and $E_{surface}$ are the energies of the isolated 3MPPA molecule and the clean surface, respectively. Calculations of the ^{31}P chemical shifts were performed using the Gauge-Including Projector Augmented Wave (GIPAW) method,[56] as implemented in the QE software package. The isotropic chemical shift δ_{iso} is defined as $\delta_{iso} = -(\sigma - \sigma_{ref})$, but in order to compare experimental and calculated chemical shifts, the isotropic shielding of the reference needs to be carefully selected. Berlinite ($AlPO_4$) with $\delta_{iso}(^{31}P) = -25.6$ ppm[57] referenced to H_3PO_4 was chosen to define $\sigma_{ref,calc}(^{31}P)$.

2.5 Adsorption experiments

Different adsorption experiments were executed, as indicated below in different subsections. For each adsorption experiment, 10 mL of Pd solution was transferred into a 20 mL glass vial containing 25 ± 0.5 mg of the adsorbent. The mixtures were stirred at 20 °C with a magnetic stirring bar at 300 rpm for a predetermined time (indicated below for each type of sorption experiment). Next, the adsorbent was separated from the aqueous solution by filtration through a 0.45 μm syringe filter (Macherey-Nagel GmbH & Co, Germany). Then, the remaining Pd concentration in the filtrate was measured using ICP-OES (Agilent Technologies 5100).

All experiments in the following subsections were performed in duplicate. The amount of Pd adsorbed per unit mass of adsorbent, q_t (mg g^{-1}), at any time t (min) is determined by eqn (2).

$$q_t = \frac{(C_0 - C_t) \cdot V}{m} \quad (2)$$

In which C_0 and C_t are the initial Pd concentration (mg L^{-1}) and the concentration at time t (min), respectively. V (L) is the volume of the solution and m (g) is the adsorbent mass.

2.5.1 Effect of initial pH value. Since the Pd speciation is strongly determined by the pH of the solution and concentration of chloride ions, stock solutions of Pd at pH 1 were prepared by dissolving $PdCl_2$ in 0.1 M HCl to ensure a fixed Cl concentration. The initial pH was adjusted using concentrated NaOH (10 M) solution or NaOH pellets. The influence of pH was studied at five different initial pH values (1.0 ± 0.1–5.0 ± 0.1). Five separate Pd solutions with a concentration of 250 mg L^{-1} were prepared as described above. After a contact time of 24 h with the adsorbent, the solution was analyzed on its Pd concentration.

2.5.2 Kinetics. A Pd solution with a 250 mg L^{-1} concentration was prepared as previously described and the pH was adjusted to pH 2.0 ± 0.1. To explore the adsorption kinetics of the adsorbents, the Pd solution was contacted with the adsorbent for different time intervals ranging from 5 min to 24 h, followed by analysis of the remaining Pd concentration in solution. For each contact time, a different vial was used containing 25 mg of sorbent and the Pd solution. The experimental data were evaluated using the non-linear form of the pseudo-first order (PFO) kinetic model (eqn (3)) and pseudo-second order (PSO) kinetic model (eqn (4)).[58]

$$q_t = q_e(1 - \exp^{-k_1 t}) \quad (3)$$

$$q_t = \frac{k_2 {q_e}^2}{1 + k_2 q_e t} \quad (4)$$

in which q_e is the adsorbed amount of Pd (mg g^{-1}) at equilibrium, q_t is the uptake at any time t (mg g^{-1}), and k_1 and k_2 are the pseudo-first order (min^{-1}) and pseudo-second order (g mg^{-1} min^{-1}) rate constants, respectively.

2.5.3 Adsorption isotherms. In order to determine the maximum adsorption capacity for Pd adsorption, Pd solutions with an initial concentration of 25 mg L^{-1} to 500 mg L^{-1} were prepared at pH 2.0 ± 0.1 and analyzed after a contact time of 24 h as described above. The experimental equilibrium data were fitted with the non-linear form of the Langmuir (eqn (5)) and Freundlich (eqn (6)) isotherm models using OriginPro 2021.[58]

$$q_e = \frac{Q_{max} K_L C_e}{(1 + K_L C_e)} \quad (5)$$

$$q_e = K_F {C_e}^{\frac{1}{n}} \quad (6)$$

in which C_e (mg L^{-1}) is the concentration of Pd in solution at equilibrium, Q_{max} (mg g^{-1}) is the maximum adsorption capacity based on the Langmuir equation, K_L (L mg^{-1}) is the Langmuir constant, K_F is the adsorption coefficient and $1/n$ is the adsorption intensity based on the Freundlich equation.

2.5.4 Regeneration efficiency. The regeneration efficiency of the adsorbents was evaluated in a adsorption–desorption–adsorption cycle. For the adsorption step, 25 mg of sorbent was brought into contact with 10 mL of a 250 mg L^{-1} Pd solution at pH 2 in a 15 mL centrifuge tube and shaken in a horizontal shaker for 30 min. Next, the adsorbents were washed three times with 10 mL water for 10 min *via* shaking. Next, the Pd loaded adsorbents were subjected to desorption by adding 10 mL of a 1 M thiourea–0.5 M HCl solution and shaking for 30 min. After washing again using the same procedure, the regenerated adsorbents were used in a subsequent adsorption step. Separation of the aqueous eluates and stripping solutions from the adsorbents was performed by centrifugation at 3000 rpm for 5 min, decantation and filtration through a 0.45 μm syringe filter, followed by analysis of the eluate on the Pd concentration. The regeneration efficiency is defined by eqn (7):

$$\text{Regeneration efficiency} = \frac{n_{\text{Pd,strip}}}{n_{\text{Pd,ads}}} \cdot 100\% \quad (7)$$

with $n_{\text{Pd,strip}}$ the molar amount of palladium in the stripping solution and $n_{\text{Pd,ads}}$ the molar amount of palladium that was initially adsorbed on the adsorbent.

2.5.5 Selective recovery from leachate of spent automotive exhaust catalyst. The selectivity towards Pd was evaluated on an acidic leachate from spent automotive exhaust catalyst. For the preparation of the leachate, a microwave-assisted leaching step in 6 M HCl was used which is described in detail elsewhere.[59,60] The pH of the leachate was adjusted to 2 using solid NaOH and afterwards filtrated through a 0.45 μm filter. Adsorption experiments were performed with 10 mL leachate and 25.0 mg adsorbent in 15 mL centrifuge tubes. After a contact time of 1 h in a horizontal shaker, the remaining metal concentrations were determined *via* ICP-OES. The distribution coefficient (K_d, mL g^{-1}) was calculated according to eqn (8):

$$K_d = \frac{V}{m} \times \frac{C_0 - C_t}{C_t} \quad (8)$$

in which V is the volume of the solution (mL), m (g) is the amount of sorbent, C_0 and C_t are the initial Pd concentration and the concentration at time t (min), respectively.

The separation factor ($SF_{Pd,M}$) indicates the selectivity of the 3MPPA sorbents towards Pd relative to other competing metal ions (M) in solution, and is defined as follows (eqn (9)):

$$SF_{Pd,M} = \frac{K_d^{Pd}}{K_d^{M}} \quad (9)$$

where K_d^{Pd} and K_d^{M} are the distribution coefficients of Pd and a competing ion, respectively.

For the quantification of the elements, the ICP-OES was calibrated in 2% HNO_3 using several calibration solutions (until 2500 μg L^{-1}) in the axial viewing direction. Independent control samples were used to check the calibration, resulting in a recovery between 90–110%. Multiple emission lines were measured for each element to verify possible interferences. All the samples were measured in different dilutions (from 5000 to 10 times) and two of the samples were spiked. When signal suppression of the internal standard (In or Lu) was more than 5%, the results were corrected. At the end of the analysis a remeasurement of the calibration blank and the highest calibration standard was performed. All calibration and control solutions used were prepared in the same matrix as the diluted samples.

3. Results and discussion

3.1 Structural and surface characterization

The nitrogen sorption isotherm of Hombikat M311 exhibits a type IV(a) isotherm with a steep capillary condensation step and a narrow H1 hysteresis loop with parallel adsorption and desorption branches in the high relative pressure range P/P_0 of 0.8–1.0 (Fig. S.2A†). This indicates the presence of large mesopores/small macropores as there is no clear saturation plateau at $P/P_0 = 1$, which is correlated to complete pore filling. The BJH analysis of the desorption branch (Fig. S.2B†) shows large mesoporous pore neck widths. Upon modification with 3MPPA, no apparent differences are observed in the shape of the isotherm and hysteresis loop (Fig. S.2A†). However, the total pore volume and BET specific surface decrease upon increasing 3MPPA concentration (Table S.1†). Compared to the native Hombikat M311, the surface area and pore volume of 3MPPA150mM have decreased most, from 0.695 to 0.614 cm^3 g^{-1} and from 300 to 207 m^2 g^{-1}, respectively.

The impact of the 3MPPA concentration on the modification degree (number of 3MPPA groups per nm^2) is shown in Table 1. The modification degree increases with increasing concentration from 0.9 # per nm^2 (20 mM) to 1.9 # per nm^2 (150 mM). The strong correlation of modification degree with concentration is in contrast to phenomena observed in the functionalization with 3-aminopropylphosphonic acid, in which the increase in surface coverage was hampered in the same concentration range and synthesis conditions.[61] The underlying reason was that, in addition to grafting of the phosphonate moiety, amine groups are involved in additional surface interactions with surface OH groups or unbound P–OH groups, due to its strong proton-acceptor and donor properties. As the acceptor–donor properties are known to be weaker for thiol groups,[62] it seems that thiol groups have less tendency to engage in additional surface interactions, allowing concentration controlled surface coverages.

Direct evidence on the presence of SH groups in the modified materials is confirmed by the presence of the S–H stretching vibration at around 2565 cm^{-1} in the DRIFT spectra of 3MPPA50 and 3MPPA150 (Fig. S.4†).[63] Given the strong similarities in the spectra at both surface coverages, and since

Table 1 Calculated modification degree based on ICP-OES analysis for Hombikat M311 modified with different concentrations of 3MPPA in water at 90 °C, expressed as number of grafted groups per nm^2 (# per nm^2) and the molar amount per g of material (mmol g^{-1})

Concentration (mM)	20	50	100	150
Modification degree (# per nm^2)	0.9	1.3	1.4	1.9
Modification degree (mmol g^{-1})	0.45	0.63	0.71	0.94

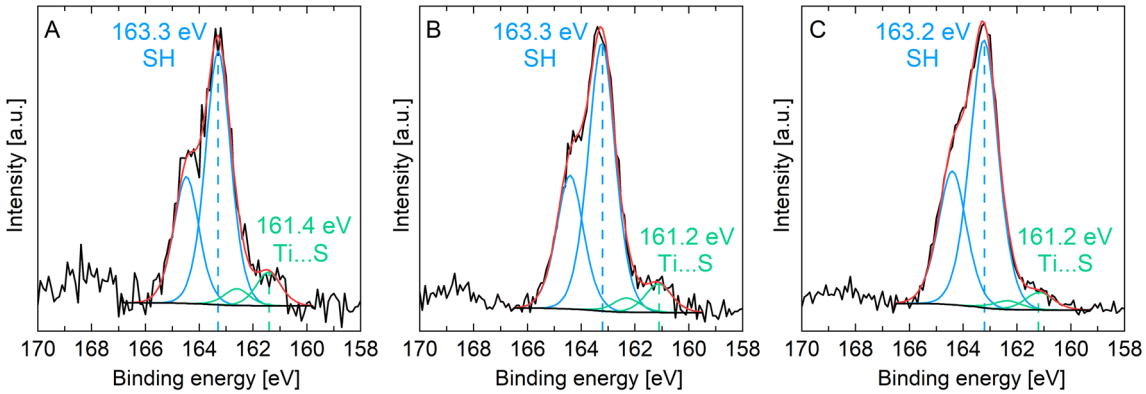

Fig. 1 S 2p XPS spectra of the 3MPPA modified Hombikat M311 adsorbents: 3MPPA20 (A), 3MPPA100 (B) and 3MPPA150 (C).

a detailed discussion on peak assignments would go beyond the scope of this work, the reader is referred to the ESI.†

XPS measurements were conducted to further deduce insights into the chemical state(s) of sulfur upon modification with 3MPPA. Fig. 1 shows the high-resolution S 2p spectra for 3MPPA20, 3MPPA100 and 3MPPA150. For the XPS survey spectra and the derived atomic concentrations, the reader is referred to Fig. S.5 and Table S.3,† respectively. The S 2p spectra consist of a broad asymmetric band owing to the spin doublet peaks of S $2p_{3/2}$ and S $2p_{1/2}$, possessing a 2 : 1 peak ratio and a 1.18 eV splitting in binding energy (BE).[64–68] Since the position of the S $2p_{3/2}$ component is commonly used in literature to deduce the chemical state of the sulfur atom, only this spin component is used for the discussion. Peak fitting of the S 2p spectra yields the presence of two components (S1 and S2). Their similar binding energies are irrespective of the modification degree (*i.e.* surface coverage). The predominant component (S1) displays the S $2p_{3/2}$ signal at a binding energy between 163.3–163.2 eV. This is in line with the range of binding energies reported for free SH groups in bulk alkanethiols (163–164 eV).[64,67] In addition, a minor S2 component is visible with the S$2p_{3/2}$ signal at a binding energy between 161.4–161.2 eV. The shift to lower binding energies indicates the presence of sulfur species in a reduced state (*e.g.* S^- or S^{2-}), and can possibly be related to thiol groups looping back to the surface through interaction with the surface.[39] Despite the lower signal-to-noise ratio for 3MPPA20, the relative contribution of the S1 component on the total intensity of the S 2p spectrum seems to increase with increasing 3MPPA concentration.

In order to provide further evidence on the looping back mechanism of thiol groups towards the TiO_2 surface, ToF-SIMS has been applied on 3MPPA20 and 3MPPA150, as a complementary technique to XPS. Fig. S.6† shows an overview of negative ToF-SIMS spectra obtained on native Hombikat M311, 3MPPA20 and 3MPPA150. Ion fragments related to the SH moiety are clearly revealed: S^- (*m*/*z*: 31.9723), $C_3H_8PO_3S^-$ (M–H, *m*/*z*: 154.9940) and TiO_2SH^- (*m*/*z*: 112.9177). Additional confirmation of these assignments is found in the absence of these *m*/*z* in the spectra of the mercapto-free analogue propylphosphonic acid grafted Hombikat M311 (3PPA20). The S/SH interaction with the titania surface is certified by the presence of TiO_2SH^- (*m*/*z*: 112.9177) and TiS^+ ion fragments (*m*/*z*: 79.9185) in the positive ToF-SIMS spectra of 3MPPA20 and 3MPPA150, as shown in Fig. 2A. Hence, sulfur atoms are involved in a Lewis-

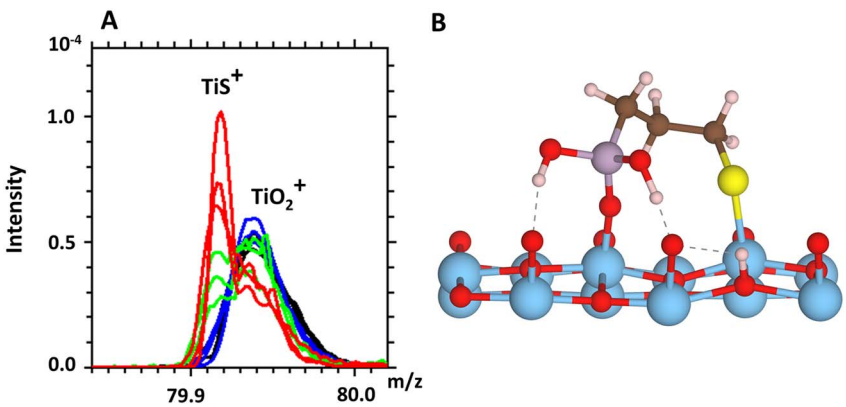

Fig. 2 (A) Positive ToF-SIMS spectra of TiS^+ overlapping with TiO_2^+, for 3MPPA20 (green), 3MPPA150 (red), 3PPA20 (blue) and Hombikat M311 (black). (B) Optimized calculated geometry of monodentate adsorbed 3MPPA on anatase (101) with dissociative S···Ti interaction. Red, cyan, pink, brown, white and yellow represent oxygen, titanium, phosphorus, carbon, hydrogen and sulfur atoms, respectively.

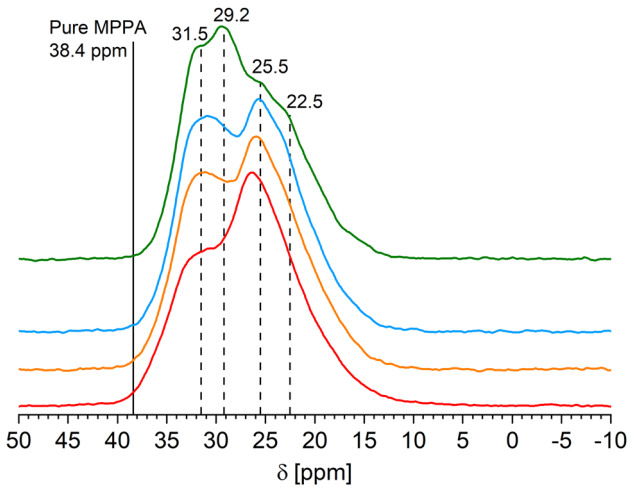

Fig. 3 ^{31}P MAS NMR spectra of Hombikat M311 modified with different concentrations of 3MPPA. 3MPPA20 (green), 3MPPA50 (blue), 3MPPA100 (orange) and 3MPPA150 (red).

type acid–base interaction with surface Ti centers, supporting the results obtained by XPS. These experimental findings are supported by DFT calculations of the 3MPPA adsorption on clean anatase (101), where both a non-dissociative (molecular) adsorption (E_{ads}: −264.02 kJ mol^{-1}) and dissociative adsorption of SH (E_{ads}: −222.75 kJ mol^{-1}) with titanium atoms on the TiO_2 surface can be formed. In these interactions, the mercaptopropyl chain is folded towards the surface resulting in a ring-type structure. The optimized geometry for a dissociative S⋯Ti interaction is depicted in Fig. 2B. For an overview of the DFT calculations, the reader is referred to the ESI (Fig. S.7, S.8 and Table S.4†).

To obtain information on the interaction of the phosphonic acid group with the surface, solid-state ^{31}P MAS NMR has been performed, as shown in Fig. 3. Pure 3MPPA shows a sharp resonance signal at 38.4 ppm (solid line, Fig. 3). Upon binding to the surface, all modified samples show a broad upfield shifted asymmetric peak between 38 and 10 ppm, originating from minor differences in the electronic environment of the phosphorus atom that are associated with different binding modes and surface conformations of 3MPPA. This is in agreement with the DFT calculations, where the sulfur group in 3MPPA has been found in intra- and inter adsorbate interactions and adsorbate–surface interactions (Fig. S.7 and S.8†). The calculated ^{31}P chemical shifts of the modelled conformations (Table S.4†) coincide with the experimental 38–10 ppm band. Nevertheless, the similar ^{31}P chemical shifts for different conformations hamper an unambiguous assignment.

For 3MPPA20, a main resonance is found at 29.2 ppm with a downfield shoulder at 31.5 ppm and less resolved upfield shoulders at 25.5 ppm and 22.5 ppm. For 3MPPA50, the 25.5 ppm signal becomes the main resonance while the relative intensity of the 29.2 ppm signal is strongly reduced and becomes an underlying signal of the 31.5 ppm signal. In addition, the 22.5 ppm signal becomes less resolved. Similar but more pronounced changes in relative intensities are observed with the ^{31}P MAS spectra of 3MPPA100 in the relative intensities between the 31.5 and 25.5 ppm signals. Upon further increasing modification degree for 3MPPA150, the 31.5 ppm signal strongly decreases in relative intensity together with a downfield shift of the 25.5 ppm signal to 26.5 ppm. One can note the transition of at least four resolved resonance signals at a low modification degree to two resolved resonance signals at a high modification degree. Furthermore, the absence of resonance signals between 10 and −10 ppm indicates that the formation of layered titanium phosphonate structures through a dissolution–precipitation reaction did not occur.[27,30]

3.2 Pd sorption

3.2.1 Effect of pH. Leachates of automotive catalytic converters, waste electrical and electronic equipment (WEEEs) and waste streams from mining often contain strong acids and high anion (*e.g.* chloride) concentrations.[6,8,69] Therefore, the impact of the pH on the adsorption capacity is studied in the region between pH 1 and 5. Furthermore, palladium is known to form stable chloro-complexes such as $PdCl_2$, $PdCl_3^-$ and $PdCl_4^{2-}$, of which their relative occurrence strongly depends on the chloride concentration and pH of the solution.[70] Therefore, during the experiments, a constant chloride concentration is maintained irrespective of the pH, ensuring that the targeted $PdCl_4^{2-}$ complex is dominant. Indeed, speciation modelling using Visual MINTEQ software[71] with the specific experimental conditions used in this study (C_{Pd} 250 mg L^{-1}, 0.1 M Cl$^-$), revealed that around 95% of all Pd is present as $PdCl_4^{2-}$ with only a minor contribution of $PdCl_3^-$ species (Fig. S.9†).

For 3MPPA50 and 3MPPA150, adsorption capacities of 56 ± 1 mg g^{-1} and 65 ± 1 mg g^{-1} are obtained, respectively, which do not change with varying pH values (Fig. 4A). This is in line with other studies describing Pd adsorption on thiol groups,[63,72–75] pointing towards an adsorption mechanism which involves the bonding between sulfur and palladium through coordination/chelation. The native Hombikat M311 shows no palladium uptake between pH 1–4 and only a slight uptake at pH 5 (*i.e.* 6 ± 0.5 mg g^{-1}). Hence, (protonated) OH groups on the titania surface contribute negligibly to the overall adsorption capacity in acidic solutions. In addition, it is of importance to assess the pH stability of the 3MPPA grafted samples as it strongly affects their performance and lifetime. The fraction of leached groups (%) was determined by measuring the amount of leached phosphorus during metal adsorption with respect to the amount of phosphorus after grafting. As shown in Fig. 4B, 3MPPA50 and 3MPPA150 exhibit 0.3–0.6% and 0.6–1.1% of phosphor leaching, respectively. Hence, these results indicate the added value of these sorbents for their implementation under harsh conditions (*i.e.* pH 1–3) that are characteristic for PGM-containing leachates.

3.3 Adsorption kinetics

The equilibrium time required to achieve the most favorable adsorption was studied. The adsorption capacity at different contact times at pH 2 and an initial Pd concentration of 250 mg L^{-1} are represented in Fig. 5. Under these conditions, an

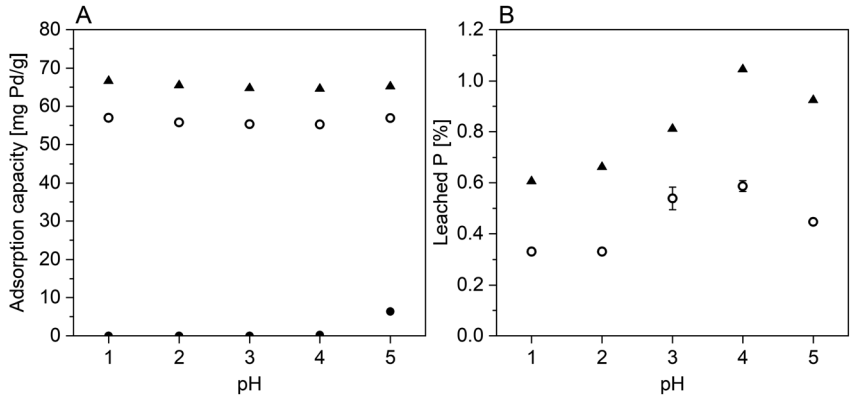

Fig. 4 Effect of pH on the adsorption capacity of Pd (mg g^{-1}, A) and the relative amount of leached phosphorus (%, B) between pH 1 and 5 for native Hombikat M311 (closed circles), 3MPPA50 (open circles) and 3MPPA150 (triangles). Adsorbent dose = 2.5 g L^{-1}, t = 24 h, C_{Pd} = 250 mg L^{-1}, 0.1 M Cl^-.

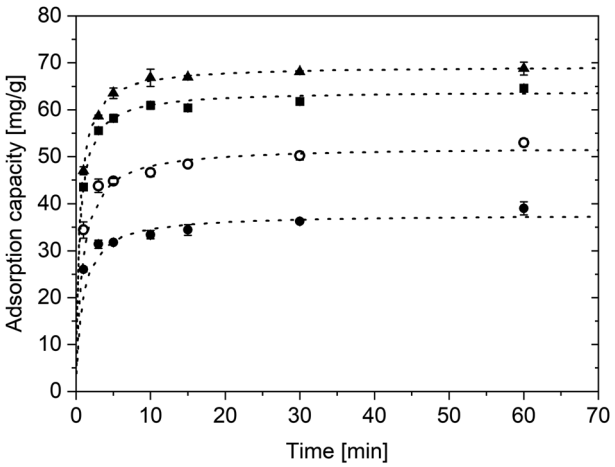

Fig. 5 Plot of non-linear pseudo-second order fit (dashed line) and experimental data points for the Pd adsorption kinetics for 3MPPA20 (closed circles), 3MPPA50 (open circles), 3MPPA100 (squares) and 3MPPA150 (triangles). C_{Pd} = 250 mg L^{-1}, adsorbent dose = 2.5 g L^{-1}, pH = 2.0.

initial Pd/functional group mole ratio of around 2 : 1 and 1 : 1 is provided for 3MPPA20 (0.9 # per nm^2) and 3MPPA150 (1.9 # per nm^2), respectively. This avoids the complete depletion of Pd at equilibrium, which would result in incorrect modeling and interpretation of the adsorption kinetics. All surface coverages exhibit a steep curve in the first 5 minutes that can be attributed to the abundant availability of active sites in the initial stage and the large mesoporous pore network that function as efficient transport channels. Eventually, all surface coverages reach more than 95% of adsorption equilibrium within 10 minutes of contact time. The experimental data were fitted according to a non-linear pseudo-first order (PFO) and pseudo-second order (PSO) kinetic model to quantify the rate of adsorption for the different surface coverages (Fig. S.10†). In order to identify the best-fit model, both the determination coefficient (R^2) value and the chi-squared (χ^2) value are commonly taken into account.[58] Based on these values, the PSO model was identified as the best-fit model, with similar adsorption rate constants k_2 (0.023–0.031 g mg^{-1} min^{-1}) within the experimental error between the different surface coverages (Table 2).

3.4 Adsorption isotherm

The adsorption performance is described using an adsorption isotherm, showing the adsorption capacity in function of the equilibrium Pd concentration (Fig. 6). To ensure equilibrium conditions, these sorption experiments were conducted for a contact time of 24 h. The adsorption isotherms are characterized by a steep, vertical increase in adsorption capacity at equilibrium concentrations of Pd at the detection limit of ICP analysis (*i.e.* 0.1 mg L^{-1}) for all surface coverages. According to the Gilles classification,[76,77] such adsorption isotherms are classified as H-type isotherms, indicating a strong affinity of the

Table 2 Parameters obtained through fitting (cal) of the experimental kinetic data (exp) with the pseudo-second order (PSO) kinetic model for Pd adsorption with C_{Pd} = 250 mg L^{-1} on 3MPPA20, 3MPPA50, 3MPPA100 and 3MPPA150

	3MPPA20	3MPPA50	3MPPA100	3MPPA150
Parameter	0.9 # per nm^2	1.3 # per nm^2	1.4 # per nm^2	1.9 # per nm^2
$q_{e,exp}$ (mg g^{-1})	39.0 ± 1.4	53.0 ± 0.8	64.6 ± 0.3	68.8 ± 1.4
$q_{e,calc}$ (mg g^{-1})	37.6 ± 1.0	52.1 ± 1.0	64.0 ± 0.7	69.3 ± 0.3
k_2 (g mg^{-1} min^{-1})	0.030 ± 0.011	0.023 ± 0.006	0.032 ± 0.007	0.031 ± 0.003
R^2	0.9971	0.9984	0.9996	0.9999
χ^2	1.715	1.494	0.680	0.135

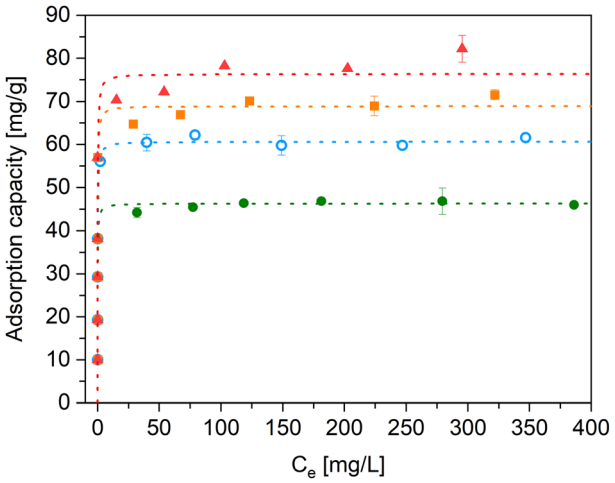

Fig. 6 Equilibrium adsorption isotherm for 3MPPA20 (green circles), 3MPPA50 (blue), 3MPPA100 (orange squares) and 3MPPA150 (red triangles). The dotted lines represent the fitted non-linear Langmuir isotherm. Adsorbent dose = 2.5 g L^{-1}, pH = 2.0, t = 24 h, 0.1 M Cl$^-$.

surface functional groups for Pd without loss of sorption efficiency at very low concentrations of Pd (<20 mg L^{-1}) in a single component system. The experimental data points were fitted with two commonly used sorption models: the Langmuir adsorption model and the Freundlich model. The resulting parameters, along with the R^2 and χ^2 values, are given in Table 3. Based on the fitting parameters, the Langmuir model was found more suitable to fit the experimental data. The plot of the Langmuir isotherm model is shown in Fig. 6 for each surface coverage. Within the fitting error, one can note that similar Langmuir constants (b) are obtained for the different surface coverages, *i.e.* ranging between 6.6–8.6 L mg^{-1}. Since this binding constant is related to the adsorption energy and affinity between palladium and the functional groups, each surface coverage has a similar binding affinity for palladium.

Based on the surface coverage of functional groups and the maximal adsorption capacity, the adsorption efficiency can be determined to examine the stoichiometry of the sorption process and the mechanism(s) of binding with Pd. Here, the adsorption efficiency is defined by the Pd/S ratio, in which "S" represents the total amount of grafted sulfur irrespective of its speciation as determined by XPS (SH, S$^-$). An overview of the calculated Pd/S ratios for each surface coverage is given in Table 4. For 3MPPA20-3MPPA100, similar calculated Pd/S ratios were obtained, *i.e.* ranging from 0.92 to 0.96, suggesting a nearly equimolar stoichiometry between S and Pd. Interestingly, for the highest surface coverage (3MPPA150), a slight decrease in the Pd/S ratio was found, *i.e.* 0.81. This observation has been verified on a reproduced SH modified sample (3MPPA150_R), where a Pd/S ratio of 0.84 was found. Previous literature studies on the adsorption of Pd and Pt on thiolated silica also described a decrease in the adsorption efficiency with increasing surface coverage, but a discussion of the possible underlying reasons was missing.[73,78]

Table 4 Calculation of the adsorption efficiency, *i.e.* the Pd/S ratio, for the different 3MPPA concentrations based on the surface coverage (mmol g^{-1}) and the maximal Pd adsorption capacity (Q_{max}, mmol g^{-1})

Sample	Mod. degr. 3MPPA (mmol g^{-1})	Q_{max}		Pd/S ratio
		mg g^{-1}	mmol g^{-1}	
3MPPA20	0.45	44–48	0.43 ± 0.02	0.96 ± 0.04
3MPPA50	0.63	60–64	0.58 ± 0.02	0.92 ± 0.03
3MPPA100	0.71	69–73	0.67 ± 0.02	0.94 ± 0.03
3MPPA150	0.94	79–83	0.76 ± 0.02	0.81 ± 0.02
3MPPA150_R	0.85	74–78	0.71 ± 0.02	0.84 ± 0.02

Explaining the decreasing adsorption efficiency is challenging as an interplay of several aspects can be present. Firstly, this phenomenon cannot be solely ascribed to the presence of Ti–S interactions, since the peak fitted S 2p spectra in Fig. 1 suggest a lower contribution of these interactions in 3MPPA150 (1.9 # per nm^2) compared to 3MPPA20 (0.9 # per nm^2), which is not in agreement with the observed Pd/S ratios. It should be noted, however, that the XPS/ToF-SIMS measurements and the DFT calculations are performed under high-vacuum and complete vacuum conditions, respectively. Under bulk aqueous conditions in the presence of palladium (during sorption) and acidic environment, competitive interactions might be present where S···Ti interactions might be relinquished in favor of S···Pd interactions, depending on the energy gain by breakage and formation of these interactions. XPS measurements on sulfur and palladium after sorption did not reveal spectral differences between the surface coverages that could explain the lower Pd/S ratio for 3MPPA150. For discussion and interpretation of the S 2p and Pd 3d XPS spectra, the reader is referred to Fig. S.11 and S.12,† respectively.

Table 3 Langmuir and Freundlich isotherm parameters for the different modification degrees for 3MPPA modified M311

Isotherm model	Parameter	3MPPA20	3MPPA50	3MPPA100	3MPPA150
Langmuir	q_{max} (mg g^{-1})	46.3 ± 2.3	60.7 ± 3.2	69.0 ± 5.2	76.4 ± 6.0
	b (L mg^{-1})	8.6 ± 2.3	6.6 ± 1.8	7.5 ± 2.5	6.7 ± 2.3
	R^2	0.8250	0.8574	0.7573	0.7611
	χ^2	30.90	56.27	132.4	174.0
Freundlich	K_F	29.7 ± 3.1	36.5 ± 4.3	40.4 ± 5.1	42.9 ± 5.3
	n	11.5 ± 2.9	9.6 ± 2.4	9.2 ± 2.3	8.2 ± 1.9
	R^2	0.6935	0.7098	0.6934	0.7462
	χ^2	54.13	114.5	167.2	184.8

Another possible explanation for the change in stoichiometry might originate from the changes in the surface conformations of 3MPPA at higher surface coverages, as supported by the ^{31}P NMR spectra (Fig. 3), showing differences in the phosphorus environments. This can result in a variety of sorption sites with different interaction energies and stoichiometry with Pd. Such surface heterogeneity is in agreement with the similarity in adsorption energies between the modeled surface conformations of 3MPPA (Table S.4†), resulting in their co-existence at the TiO_2 surface.

Next, a high surface coverage (1.9 # per nm^2) is likely to result in a smaller adjacent distance between stretched mercaptopropyl chains, creating sorption sites where bidentate coordinating modes (ML_2 type interactions) might occur upon sorption. However, the calculated Pd/S ratio of around 0.8 instead of 0.5 supports the presence of a heterogenous surface with the co-existence of ML and ML_2 interactions upon sorption. It should be noted that the coordination might also be influenced by steric–repulsive interactions which might occur between a pre-occupied sorption site and an adjacent free sorption site. Experimental and computational studies report that a $PdCl_4^{2-}$ complex has an effective size of 5.5 Å.[79,80] As such, we could envisage that steric hindering can occur between adjacent 3MPPA groups with S⋯S distances below 5.5 Å. Table S.5† shows the calculated S⋯S distances obtained from the DFT calculations of adjacent 3MPPA groups with SH groups involved in hydrogen bonding (SH⋯H) or as free/non-interacting groups. Although a feasible explanation for the decreased adsorption efficiency at 3MPPA coverage of 1.9 # per nm^2, one should remark that these are static distances obtained in the absence of water and at zero Kelvin, while under more realistic conditions, these distances will vary due to the high flexibility of alkyl chains. Taking into account the aforementioned discussion on possible reasons for the difference in Pd/S ratio, it is difficult to prove or disprove either hypotheses, neither its relative contribution to the sorption mechanism and performance.

3.5 Regeneration efficiency for single-element solution of palladium

A high regeneration efficiency is an important property for a metal scavenger, enabling a quantitative elution and high preconcentration factor for Pd in subsequent processing. In addition, from economical point of view, this increases the cost-efficiency and the time-on-stream of the adsorbent material. Various eluants including HNO_3, HCl, EDTA and (acidified) thiourea have been reported for the elution of PGMs.[78,81,82] In the optimization and choice of the elution conditions, a balance between negligible adsorbent degradation and elution strength have to be considered. Both HNO_3 and HCl display weak eluting properties, and only at very high concentrations (>6 M), an increase in the elution strength is observed.[73,78,82] These observations reflect the high affinity between PGMs and thiol functional groups.

In turn, the oxidizing properties of HNO_3 can potentially result in the formation of oxidized SO_x groups,[78] causing a pronounced loss in adsorption capacity in subsequent adsorption steps due to the low affinity of oxygen donor atoms for PGMs. In general, such high acid concentrations can have a detrimental impact on the adsorbent properties, owing to a pronounced loss of functional groups and/or changes in the structural properties of the TiO_2 support. In general, acidified aqueous thiourea solutions, using HCl as inorganic acid, exhibit the best eluting power. Therefore, this work evaluated palladium desorption with a 0.5 M HCl–1 M thiourea aqueous solution. The desorption efficiency is calculated as the amount of desorbed palladium relative to the amount of palladium initial adsorbed, both expressed in mg g^{-1}. The ad/desorption capacities (Q_t) for all materials with different modification degrees are shown in Fig. 7. Due to the difference in experimental set-up (*i.e.* shaking of solutions instead of stirring) to maximally recover the material between the different ad/desorption steps, the Q_t values are not comparable with the above reported adsorption results of the Pd kinetics and isotherms (Fig. 5 and 6). With increasing surface coverage from 3MPPA20 to 3MPPA150, a decrease in desorption efficiency from around 95 to 75% was observed. In the 2nd adsorption step, taking the measurement error into account, the same amount of palladium was adsorbed as previously desorbed. These results show the potential of 3MPPA grafted TiO_2 materials forming strong coordinative bonds with sulfur atoms, while allowing efficient desorption. We envision that further optimization can be achieved by altering the desorption protocol (*e.g.* contact time, thiourea and/or HCl concentration).

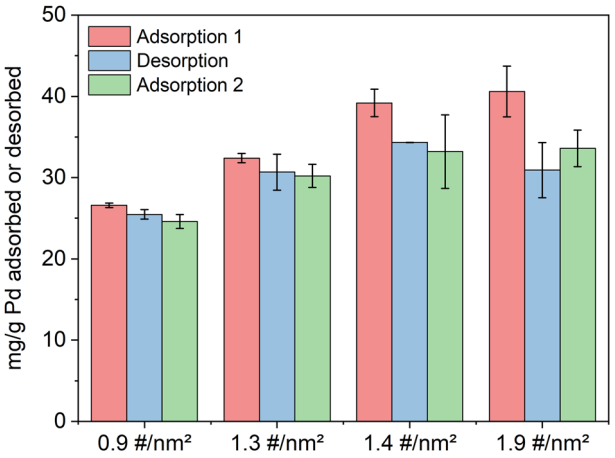

Fig. 7 Pd adsorption, recovery and adsorption capacity (mg g^{-1}) in consecutive steps. Adsorbent dose = 2.5 g L^{-1}, pH = 2.0, t = 30 min, C_{Pd} = 250 mg L^{-1}.

3.6 Selectivity in acidic leachate from spent automotive catalyst

To study the application potential and performance of the developed sorbent materials for the recovery of Pd in relevant conditions with a multitude of co-existing base metals in high concentrations, the adsorption performance was evaluated in an acidic leachate originating from spent automotive ceramic catalysts. The initial elemental composition of the leachate is

Table 5 Concentrations (mg L^{-1}) of metals present in the spent automotive catalyst acidic leachate as determined by ICP-OES, represented in order of decreasing concentration[a]

Metal	Al	Ce	Mg(1)	Ba	La	Fe	Pt	Pd
mg L^{-1}	12375	2605	1930	486	201	170	170	152
±	50	60	0	20	6	6	6	1
Metal	Zr	Ca	Y	Nd	Ti	Cr	Rh	Cu
mg L^{-1}	108	44.4	39.6	36.8	29.1	15.6	8.5	2.0
±	1	1.6	2.9	3.1	1.2	0.6	0.4	0.2

[a] Reported values and standard errors are based on four measurements, except for (1) that is based on two measurements.

presented in Table 5. The leachate was characterized by a high anion concentration (1.1 M Cl^-) and contains Al, Ce, Mg and Ba as predominant elements.

In order to study the impact of the introduction of grafted sulfur-containing functional groups, an increasing modification degree, and its possible correlations to differences in surface chemistry (*e.g.* different surface conformations, S speciation, *etc.*), adsorption experiments have been performed for all materials, covering the different surface coverages next to the native TiO_2 mesoporous powder (Hombikat M311). Given the very large concentration range (between 2 mg L^{-1} to 12 g L^{-1}) of the composing metals in the acidic leachate, both the distribution coefficient (K_d) and adsorption capacity (Q_t, mmol g^{-1}) have been calculated for all elements and depicted in Fig. S.13 and S.14,† respectively. This reveals that Fe, Pt and Pd are the major elements being adsorbed, and a plot of the K_d and Q_t values is shown in Fig. 8.

As expected based on the sorption experiments on native Hombikat M311 with a single element Pd solution, a negligible adsorption for palladium was also found for the acidic leachate solution. Noticeably, native Hombikat M311 exhibits a distinctive selectivity for the adsorption of Fe^{3+}, given the high K_d (750 mL g^{-1}) and Q_t (0.82 mmol g^{-1}). Despite a strongly reduced adsorption of cations on TiO_2 at pH < 3, as supported by previous studies[83–85] and evidenced by the negligible adsorption of the other composing metals of the leachate (pH = 2) in this work, these results reveal a strong affinity of TiO_2 surface sites for Fe^{3+}. The feasibility of the selective removal of Fe^{3+} from an acidic leachate has been demonstrated recently by adsorption on mesoporous titania microspheres, developed by vibrational droplet coagulation.[86] For 3MPPA20 (0.9 # per nm^2), the selectivity and affinity for Fe is reduced significantly (K_d = 275 mL g^{-1}, Q_t = 0.52 mmol g^{-1}). An increase in surface coverage of 3MPPA results in a further decrease in Fe adsorption, reaching a K_d and Q_t value of 82 mL g^{-1} and 0.21 mmol g^{-1} for 3MPPA150 (1.9 # per nm^2), respectively. A plausible reason is the reduced amount of surface interaction sites with which the Fe ions can interact after 3MPPA grafting. In addition, after grafting, TiO_2 surface sites might also be involved in surface interactions with the phosphoryl group (P–OH, P=O) or the thiol group, which might reduce their ability to interact with Fe ions.

Pd and Pt are present in the same order of magnitude in the leachate solution, *i.e.* 170 mg L^{-1} and 152 mg L^{-1}, respectively. It is well-known that they experience competitive adsorption for available SH sites. An increase in K_d value and adsorption capacity is observed for Pd with increasing surface coverage from 3MPPA20 (0.9 # per nm^2) to 3MPPA150 (1.9 # per nm^2), ranging from 125 mL g^{-1} to 530 mL g^{-1} and 0.14 mmol g^{-1} to 0.32 mmol g^{-1}. Compared to the adsorption capacity of 3MPPA150 of 0.76 mmol g^{-1} in a single Pd solution (Section 3.4), a 55–60% lower capacity is obtained, illustrating the occurrence of competitive interactions during adsorption under real conditions. Clearly, the developed sorbents have a stronger affinity for Pd compared to Pt for each surface coverage, obtaining K_d values between 45–113 mL g^{-1} for the latter. Given the competitive sorption behavior of Pd and Pt for the same binding sites, it is of interest to evaluate the separation factor (SF) of Pd relative to Pt (Table S.6†) as function of the surface coverage. Separation factors of 2.8 ± 0.1 and 4.7 ± 1.2 are found for a surface coverage of 0.9 # per nm^2 and 1.9 # per nm^2, respectively, revealing an increase in the separation power of Pd–Pt at higher surface coverages.

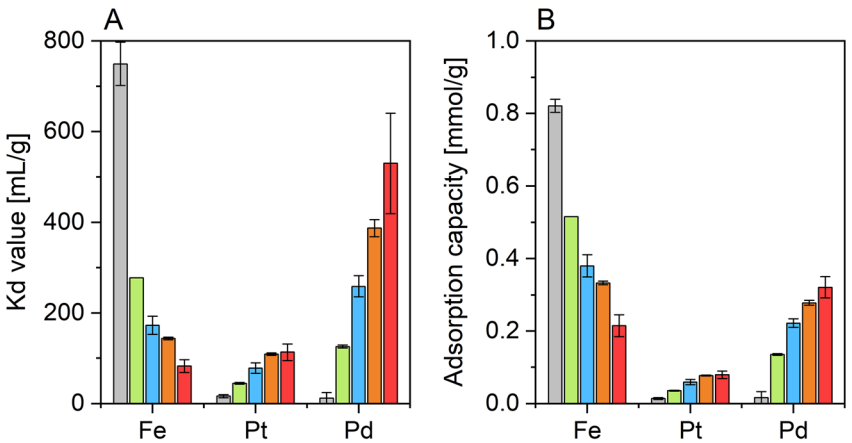

Fig. 8 (A) Distribution coefficient values (K_d) and (B) adsorption capacity (mmol g^{-1}) for Fe, Pd and Pt in the automotive catalyst acidic leachate upon adsorption on native Hombikat M311 (grey) and 3MPPA grafted Hombikat M311 with different surface coverages. 3MPPA20 (green), 3MPPA50 (blue), 3MPPA100 (orange) and 3MPPA150 (red).

Table 6 Comparison of Pd adsorption capacities and kinetics by different adsorbents reported in literature[a]

Adsorbent	pH or acid	Q_{max} (mmol g^{-1})	Eq. time (min)	k_2 (g mg^{-1} min)	Ref.
MPTMS functionalized SBA-15	4	1.60	100	—	63
MPTMS functionalized SBA-15	1.5–4	1.78	30	—	73
MPTMS functionalized SiO_2 coated graphene oxide	3.5	3.95	100	0.0069	72
MPTMS functionalized SBA-15	3	1.37	15	—	87
Thiourea modified magnetic nanoparticles	2	1.05	30	—	82
Thioctic acid functionalized ZrO_2	0.3	0.06	200	0.0218	45
Cu_xS_y/carbon composites	1.5	0.95	50	0.0126	88
Thiourea functionalized chitosan	2	1.05	150	0.0005	89
Dithiocarbamate functionalized cellulose	0.2 M HCL	2.84	90	0.0119	90
2,5-Dimercapto-1,3,4-thiodiazole functionalized chitosan	0–5	0.16	30	0.0037	91
Thiourea functionalized pine-sawdust biosorbent	2 M HCL	1.70	>360	0.0026	92
Crosslinked multidentate thia-crown ethers	6 M HCL	2.00	360	0.00035	93
p-Sulfonatothiacalix[*n*]arene impregnated Amberlite XAD-7	1–4	1.27	180	0.0022	94
2	0.1–8 M HCL	0.41	150	0.00032	95
Duolite GT-73 resin (thiol)	0.1–3M HCL	0.20	350	—	96
Lewatit TP-214 resin (thiourea)	0.1–3 M HCL	1.16	50	—	96
Spheron Thiol 1000	2	0.95	480	—	97
Bisthiourea modified persimmon tannin	1	1.72	720	—	98
1,2-Ethylenedisulfide modified chitosan	0.01–5 M HCL	2.33	10	—	99
Bis(isopentyl)-sulfide-impregnated α-MnO_2 nanorods	2	0.77	90	0.0020	100
Zr-based MOF with 2,6-bis(allylsulfanyl) terephthalic acid linker	3 M HNO_3	0.42	60	—	101
Quadrasil MP[b]	2	0.88	10	—	102
3-Mercaptopropylphosphonic acid functionalized TiO_2	2	0.76	15	0.03	This work

[a] MPTMS = mercaptopropyltrimethoxysilane. [b] Measurements and reported results obtained within this PhD, while the reference gives background on the material and supplier.

3.7 Benchmarking with other adsorbents on Pd recovery

To compare the performance of 3MPPA grafted TiO_2 with Pd scavengers containing sulfur functional groups, the most relevant studies from literature were collected and summarized in Table 6. Four different classes of support materials can be identified, being silica, metal oxides, (bio)polymers and carbon composites. Admittedly, evaluating the performance of a Pd scavenger is a multi-faceted study, as diverse properties should be taken into account (*e.g.* stability, capacity, kinetics, reusability in multiple cycles). Two parameters were selected in the benchmarking, the maximal adsorption capacity (Q_{max}) and the equilibrium time to reach full capacity, of which both are collected in Fig. 9 and Table 6 for each study. The (bio)polymer-based Pd adsorbents (green dots) exhibit a broad range of Q_{max} values (0.2–2 mmol g^{-1}), with the majority having equilibrium times higher than 100 min, with some exceptions with equilibrium times in the range of 10 min. Silica materials (blue dots) are characterized by Q_{max} values above 0.9 mmol g^{-1} and with the fastest kinetics reaching equilibrium conditions below 100 min and as low as 10 min. Lastly, metal oxides (orange dots) reveal strong similarities with silica materials but currently possess lower Q_{max} values (0.1–1.0 mmol g^{-1}). Clearly, the

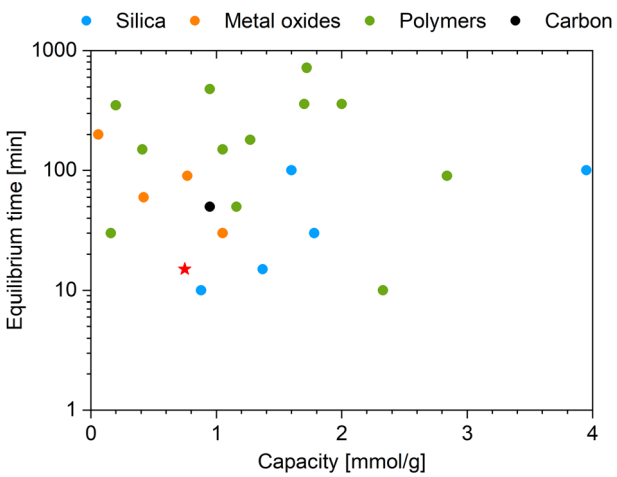

Fig. 9 Plot of the maximal palladium adsorption capacity (mmol g^{-1}) and equilibrium time (min) for different classes of sulfur-containing adsorbents (silica materials, metal oxides, (bio)polymers and carbon-based). The plotted data points are based on the adsorption capacities and equilibrium times depicted in Table 6. The red star represents 3MPPA150 (this study).

developed 3MPPA adsorbent (red star) has among the fastest kinetics compared to other studies available in literature, being similar to the silica materials while having the advantage in offering flexible synthetic control and more benign modification conditions. The major drawback is the co-adsorption of Fe on the titania support, and therefore, streams containing this metal ion should be avoided.

4. Conclusion

This work reports an aqueous-based modification method of 3-mercaptopropylphosphonic acid (3MPPA) grafted mesoporous TiO_2, contributing towards the development of selective Pd scavengers. During synthesis, the 3MPPA concentration has been varied to study the impact on the surface coverage, and its correlation with the palladium sorption performance in acidic solutions. Concentration-controlled surface coverages were obtained, ranging from 0.9 to 1.9 groups per nm^2.

For surface coverages between 0.9–1.4 # per nm^2, a nearly equimolar stoichiometry between palladium and sulfur was found (0.81 < Pd/S ratio < 1), suggesting that the majority of sorption sites were available for coordination with Pd. Furthermore, a maximum adsorption capacity of 0.76 mmol g^{-1} was attained for the highest surface coverage. The grafted samples exhibited excellent hydrolytic stability with no loss in adsorption performance at lower pH values (1–2) in single-element solutions. The relative loss of functional groups was well below 1% for an exposure time of 24 h at pH 1.

The developed sorbent was evaluated in relevant conditions, showing a high selectivity and adsorption capacity towards Pd (K_d = 125–530 mL g; Q_t = 0.14–0.32 mmol g^{-1}) during sorption in an acidic leachate from a spent automotive exhaust catalyst. Controlling the surface coverage of 3MPPA groups is important for the selectivity towards Pd, given the selective and strong co-adsorption of Fe(III) on TiO_2 support. By increasing the surface coverage from 0.9 to 1.9 # per nm^2, the separation factor of Pd with respect to Fe could be increased from 0.5 to 6.4.

Author contributions

Nick Gys: conceptualization, methodology, validation, investigation, writing-original draft, visualization. Bram Pawlak (^{31}P-NMR): methodology, validation, investigation, writing-review & editing. Léon Luntadila Lufungula (DFT): methodology, validation, investigation, writing-review & editing, visualization. Kristof Marcoen (ToF-SIMS): methodology, validation, investigation, writing-review & editing, visualization. Kenny Wyns: methodology, validation, investigation. Kitty Baert (XPS): methodology, validation, investigation, visualization. Thomas Abo Atia: methodology, validation, investigation. Jeroen Spooren: methodology, validation, writing-review & editing. Peter Adriaensens (^{31}P-NMR): methodology, writing-review & editing, supervision. Frank Blockhuys (DFT): methodology, validation, investigation, writing-review & editing, supervision. : methodology, writing-review & editing, supervision. Vera Meynen: conceptualization, methodology, writing-review & editing, supervision. Steven Mullens: conceptualization, methodology, writing-review & editing, supervision. Bart Michielsen: conceptualization, methodology, writing-review & editing, supervision.

Conflicts of interest

There are no conflicts of interest to declare.

Acknowledgements

This work is supported by the Research Foundation Flanders (FWO) and Hasselt University *via* the Hercules project AUHL/15/2 – GOH3816N. Part of the presented work was executed within the PLATIRUS project, which has received funding from the European Union's Horizon 2020 research and innovation program under grant agreement No 730224. This work reflects only the author's views and the agency is not responsible for any use that may be made of the information it contains. The authors are grateful to all project partners for discussions and input, and in particular to Monolithos Ltd (Athens. Greece) for providing the spend automotive catalyst material used in this work. V. Meynen acknowledges the Research Foundation-Flanders (FWO) for project K801621N. All calculations were performed using the Hopper HPC infrastructure at the CalcUA core facility of the University of Antwerp, a division of the Flemish Supercomputer Center VSC, funded by the Hercules Foundation, the Flemish Government (department EWI) and the University of Antwerp. Furthermore, the authors would like to acknowledge S. Defossé and K. Leyssens for the N_2 sorption measurements, J. Lievens and A. Deibe Varela for the Pd sorption experiments, K. Duyssens and W. Brusten for the ICP measurements and M. Mertens for the XRD measurements.

References

1 C. R. M. Rao and G. S. Reddi, Platinum group metals (PGM); occurrence, use and recent trends in their determination, *Trends Anal. Chem.*, 2000, **19**, 565–586.
2 G. M. Mudd, S. M. Jowitt and T. T. Werner, Global platinum group element resources, reserves and mining – A critical assessment, *Sci. Total Environ.*, 2018, **622–623**, 614–625.
3 European Commission, *Critical Raw Materials Resilience: Charting a Path towards greater Security and Sustainability*, 2020, DOI: 10.1007/978-3-030-40268-6_9.
4 J. Spooren, *et al.*, Near-zero-waste processing of low-grade, complex primary ores and secondary raw materials in Europe: technology development trends, *Resour., Conserv. Recycl.*, 2020, **160**, 104919.
5 R. M. Izatt, S. R. Izatt, R. L. Bruening, N. E. Izatt and B. A. Moyer, Challenges to achievement of metal sustainability in our high-tech society, *Chem. Soc. Rev.*, 2014, **43**, 2451–2475.
6 H. B. Trinh, J. chun, Y. j. Suh and J. Lee, A review on the recycling processes of spent auto-catalysts: Towards the development of sustainable metallurgy, *Waste Manage.*, 2020, **114**, 148–165.

7 M. Rzelewska and M. Regel-Rosocka, Wastes generated by automotive industry - Spent automotive catalysts, *Phys. Sci. Rev.*, 2019, **3**, 1–27.
8 Y. Ding, *et al.*, Recovery of precious metals from electronic waste and spent catalysts: A review, *Resour., Conserv. Recycl.*, 2019, **141**, 284–298.
9 S. Sharma, A. S. Krishna Kumar and N. Rajesh, A perspective on diverse adsorbent materials to recover precious palladium and the way forward, *RSC Adv.*, 2017, **7**, 52133–52142.
10 H. Zheng, Y. Ding, Q. Wen, B. Liu and S. Zhang, Separation and purification of platinum group metals from aqueous solution: Recent developments and industrial applications, *Resour., Conserv. Recycl.*, 2021, **167**, 105417.
11 R. Ruhela, A. K. Singh, B. S. Tomar and R. C. Hubli, Separation of palladium from high level liquid waste - A review, *RSC Adv.*, 2014, **4**, 24344–24350.
12 S. Soltani, N. Khanian, U. Rashid and T. S. Yaw Choong, Fundamentals and recent progress relating to the fabrication, functionalization and characterization of mesostructured materials using diverse synthetic methodologies, *RSC Adv.*, 2020, **10**, 16431–16456.
13 V. Meynen, H. Castricum and A. Buekenhoudt, Class II Hybrid Organic-inorganic Membranes Creating New Versatility in Separations, *Curr. Org. Chem.*, 2014, **18**, 2334–2350.
14 K. Turke, *et al.*, Amine-Functionalized Nanoporous Silica Monoliths for Heterogeneous Catalysis of the Knoevenagel Condensation in Flow, *ACS Omega*, 2021, **6**, 425–437.
15 S. P. Pujari, L. Scheres, A. T. M. Marcelis and H. Zuilhof, Covalent surface modification of oxide surfaces, *Angew. Chem., Int. Ed.*, 2014, **53**, 6322–6356.
16 E. Asenath Smith and W. Chen, How To Prevent the Loss of Surface Functionality Derived from Aminosilanes, *Langmuir*, 2008, **24**, 12405–12409.
17 M. Zhu, M. Z. Lerum and W. Chen, How to prepare reproducible, homogeneous, and hydrolytically stable aminosilane-derived layers on silica, *Langmuir*, 2012, **28**, 416–423.
18 M. Etienne and A. Walcarius, Analytical investigation of the chemical reactivity and stability of aminopropyl-grafted silica in aqueous medium, *Talanta*, 2003, **59**, 1173–1188.
19 A. L. T. Pham, D. L. Sedlak and F. M. Doyle, Dissolution of mesoporous silica supports in aqueous solutions: Implications for mesoporous silica-based water treatment processes, *Appl. Catal., B*, 2012, **126**, 258–264.
20 D. V. Okhrimenko, *et al.*, Hydrolytic Stability of 3-Aminopropylsilane Coupling Agent on Silica and Silicate Surfaces at Elevated Temperatures, *ACS Appl. Mater. Interfaces*, 2017, **9**, 8344–8353.
21 P. H. Mutin, G. Guerrero and A. Vioux, Organic-inorganic hybrid materials based on organophosphorus coupling molecules: From metal phosphonates to surface modification of oxides, *C. R. Chim.*, 2003, **6**, 1153–1164.
22 C. Queffélec, M. Petit, P. Janvier, D. A. Knight and B. Bujoli, Surface Modification Using Phosphonic Acids and Esters, *Chem. Rev.*, 2012, **112**, 3777–3807.
23 P. H. Mutin and G. Guerrero, Hybrid materials from organophosphorus coupling molecules, *J. Mater. Chem.*, 2005, **15**, 3761–3768.
24 R. Boissezon, J. Muller, V. Beaugeard, S. Monge and J. J. Robin, Organophosphonates as anchoring agents onto metal oxide-based materials: Synthesis and applications, *RSC Adv.*, 2014, **4**, 35690–35707.
25 G. Guerrero, J. G. Alauzun, M. Granier, D. Laurencin and P. H. Mutin, Phosphonate coupling molecules for the control of surface/interface properties and the synthesis of nanomaterials, *Dalton Trans.*, 2013, **42**, 12569–12585.
26 A. Cattani-Scholz, Functional Organophosphonate Interfaces for Nanotechnology: A Review, *ACS Appl. Mater. Interfaces*, 2017, **9**, 25643–25655.
27 A. Roevens, *et al.*, Revealing the influence of the solvent in combination with temperature, concentration and pH on the modification of TiO2 with 3PA, *Mater. Chem. Phys.*, 2016, **184**, 324–334.
28 A. Roevens, *et al.*, Aqueous or solvent based surface modification: The influence of the combination solvent – organic functional group on the surface characteristics of titanium dioxide grafted with organophosphonic acids, *Appl. Surf. Sci.*, 2017, **416**, 716–724.
29 M. Tassi, *et al.*, A detailed investigation of the microwave assisted phenylphosphonic acid modification of P25 TiO2, *Adv. Powder Technol. Adv. Powder Technol.*, 2017, **28**, 236–243.
30 M. Tassi, G. Reekmans, R. Carleer and P. Adriaensens, Fully quantitative description of hybrid TiO2 nanoparticles by means of solid state 31P NMR, *Solid State Nucl. Magn. Reson.*, 2016, **78**, 50–55.
31 C. Di Valentin and D. Costa, Anatase TiO 2 surface functionalization by alkylphosphonic acid: A DFT+D study, *J. Phys. Chem. C*, 2012, **116**, 2819–2828.
32 M. Nilsing, S. Lunell, P. Persson and L. Ojamäe, Phosphonic acid adsorption at the TiO_2 anatase (1 0 1) surface investigated by periodic hybrid HF-DFT computations, *Surf. Sci.*, 2005, **582**, 49–60.
33 D. Geldof, *et al.*, Binding modes of phosphonic acid derivatives adsorbed on TiO2surfaces: Assignments of experimental IR and NMR spectra based on DFT/PBC calculations, *Surf. Sci.*, 2017, **655**, 31–38.
34 R. Luschtinetz, J. Frenzel, T. Milek and G. Seifert, Adsorption of phosphonic acid at the tio$_2$ anatase (101) and rutile (110) surfaces, *J. Phys. Chem. C*, 2009, **113**, 5730–5740.
35 R. Luschtinetz, S. Gemming and G. Seifert, Anchoring functional molecules on Tio2 surfaces: A comparison between the carboxylic and the phosphonic acid group, *Eur. Phys. J. Plus*, 2011, **126**, 1–13.
36 G. Ramanath, *et al.*, Tuning of noble metal work function with organophosphonate nanolayers, *Appl. Phys. Lett.*, 2014, **105**, 081601.

37 S. J. Wilkins, T. Paskova and A. Ivanisevic, Modified surface chemistry, potential, and optical properties of polar gallium nitride *via* long chained phosphonic acids, *Appl. Surf. Sci.*, 2015, **327**, 498–503.
38 M. Kwan, T. Cardinal, P. H. Mutin and G. Ramanath, Work function tuning at Au-HfO2 interfaces using organophosphonate monolayers, *Appl. Phys. Lett.*, 2016, **108**, 191607.
39 M. Kwan, T. Cardinal, P. H. Mutin and G. Ramanath, Molecular length effect on work function shifts at copper-organophosphonate-hafnia interfaces, *Appl. Phys. Lett.*, 2017, **110**, 5.
40 M. Kwan, R. Winter, P. H. Mutin, M. Eizenberg and G. Ramanath, Tailoring Al-SiO2 interfacial work function using an organophosphonate nanolayer, *Appl. Phys. Lett.*, 2017, **111**, 5.
41 L. Etgar, *et al.*, Design and development of novel linker for PbS quantum dots/TiO2 mesoscopic solar cell, *ACS Appl. Mater. Interfaces*, 2011, **3**, 3264–3267.
42 D. Aldakov, *et al.*, Mercaptophosphonic acids as efficient linkers in quantum dot sensitized solar cells, *J. Mater. Chem. A*, 2015, **3**, 19050–19060.
43 D. Aldakov, *et al.*, Mercaptophosphonic acids as efficient linkers in quantum dot sensitized solar cells, *J. Mater. Chem. A*, 2015, **3**, 19050–19060.
44 S. Anthérieu, G. G. Florence Brodard-Séverac and P. H. Mutin, Self-Assembled Monolayers of 12-Mercaptododecylphosphonic Acid on Titania Particles; Application to the Extraction of Heavy Metals, *Mater. Res. Soc. Symp. Proc.*, 2005, **847**, 1–6.
45 Q. A. Trieu, *et al.*, Interfacial study of surface-modified ZrO2 nanoparticles with thioctic acid for the selective recovery of palladium and gold from electronic industrial wastewater, *Sep. Purif. Technol.*, 2020, **237**, 116353.
46 L. S. Dake and R. J. Lad, Ultrathin Al Overlayers on Clean and K-Covered TiO 2 (110) Surfaces, *Surf. Sci. Spectra*, 1996, **4**, 232–245.
47 X. Wu, F. Wiame, V. Maurice and P. Marcus, Effects of water vapour on 2-mercaptobenzothiazole corrosion inhibitor films deposited on copper, *Corros. Sci.*, 2021, **189**, 1–5.
48 I. Kostanovskiy, F. O. Schumann, Y. Aliaev, Z. Wei and J. Kirschner, Core-resonant double photoemission from palladium films, *J. Phys.: Condens. Matter*, 2016, **28**, 15601.
49 P. Giannozzi, *et al.*, QUANTUM ESPRESSO: A modular and open-source software project for quantum simulations of materials, *J. Phys.: Condens. Matter*, 2009, **21**, 395502.
50 Z. Wu and R. E. Cohen, More accurate generalized gradient approximation for solids, *Phys. Rev. B: Condens. Matter Mater. Phys.*, 2006, **73**, 2–7.
51 F. Tran, R. Laskowski, P. Blaha and K. Schwarz, Performance on molecules, surfaces, and solids of the Wu-Cohen GGA exchange-correlation energy functional, *Phys. Rev. B: Condens. Matter Mater. Phys.*, 2007, **75**, 1–14.
52 P. E. Blöchl, Projector augmented-wave method, *Phys. Rev. B*, 1994, **50**, 17953–17979.
53 S. Grimme, Semiempirical GGA-Type Density Functional Constructed with a Long-Range Dispersion Correction, *J. Comput. Chem.*, 2006, **32**, 174–182.
54 V. Barone, Role and Effective Treatment of Dispersive Forces in Materials: Polyethylene and Graphite Crystals as Test Cases, *J. Comput. Chem.*, 2009, **32**, 174–182.
55 T. Björkman, CIF2Cell: Generating geometries for electronic structure programs, *Comput. Phys. Commun.*, 2011, **182**, 1183–1186.
56 C. J. Pickard and F. Mauri, All-electron magnetic response with pseudopotentials: NMR chemical shifts, *Phys. Rev. B: Condens. Matter Mater. Phys.*, 2001, **63**, 2451011–2451013.
57 D. Müller, E. Jahn, G. Ladwig and U. Haubenreisser, High-resolution solid-state 27Al and 31P NMR: correlation between chemical shift and mean Al-O-P angle in AlPO4 polymorphs, *Chem. Phys. Lett.*, 1984, **109**, 332–336.
58 H. N. Tran, S. J. You, A. Hosseini-Bandegharaei and H. P. Chao, Mistakes and inconsistencies regarding adsorption of contaminants from aqueous solutions: A critical review, *Water Res.*, 2017, **120**, 88–116.
59 J. Spooren and T. Abo Atia, Combined microwave assisted roasting and leaching to recover platinum group metals from spent automotive catalysts, *Miner. Eng.*, 2020, **146**, 106153.
60 T. Abo Atia, W. Wouters, G. Monforte and J. Spooren, Microwave chloride leaching of valuable elements from spent automotive catalysts: Understanding the role of hydrogen peroxide, *Resour., Conserv. Recycl.*, 2021, **166**, 105349.
61 N. Gys, *et al.*, Experimental and computational insights into the aminopropylphosphonic acid modification of mesoporous TiO2 powder: The role of the amine functionality on the surface interaction and coordination, *Appl. Surf. Sci.*, 2021, **566**, 150625.
62 G. Desiraju and T. Steiner, *The Weak Hydrogen Bond: In Structural Chemistry and Biology*, Oxford University Press, 2001, DOI: **10.1093/acprof:oso/9780198509707.001.0001**.
63 T. Kang, Y. Park and J. Yi, Highly selective adsorption of Pt2+ and Pd2+ using thiol-functionalized mesoporous silica, *Ind. Eng. Chem. Res.*, 2004, **43**, 1478–1484.
64 D. G. Castner, K. Hinds and D. W. Grainger, X-ray photoelectron spectroscopy sulfur 2p study of organic thiol and bisulfide binding interactions with gold surfaces, *Langmuir*, 1996, **12**, 5083–5086.
65 J. Christopher Love, *et al.*, Formation and structure of self-assembled monolayers of alkanethiolates on palladium, *J. Am. Chem. Soc.*, 2003, **125**, 2597–2609.
66 G. Corthey, A. A. Rubert, G. A. Benitez, M. H. Fonticelli and R. C. Salvarezza, Electrochemical and X-ray photoelectron spectroscopy characterization of Alkanethiols adsorbed on palladium surfaces, *J. Phys. Chem. C*, 2009, **113**, 6735–6742.
67 K. McEleney, C. M. Crudden and J. H. Horton, X-ray photoelectron spectroscopy and the auger parameter as tools for characterization of silica-supported pd catalysts for the suzuki-miyaura reaction, *J. Phys. Chem. C*, 2009, **113**, 1901–1907.

68 C. Vericat, *et al.*, Self-assembled monolayers of thiolates on metals: A review article on sulfur-metal chemistry and surface structures, *RSC Adv.*, 2014, **4**, 27730–27754.
69 M. Sethurajan, *et al.*, Recent advances on hydrometallurgical recovery of critical and precious elements from end of life electronic wastes - a review, *Crit. Rev. Environ. Sci. Technol.*, 2019, **49**, 212–275.
70 K. Folens, S. Van Hulle, F. Vanhaecke and G. Du Laing, Chemical fractionation and speciation modelling for optimization of ion-exchange processes to recover palladium from industrial wastewater, *Water Sci. Technol.*, 2016, **73**, 1738–1745.
71 J. P. Gustafsson, *Visual MINTEQ Program Version 3.1*, 2015, available at: **https://vminteq.lwr.kth.se/**.
72 M. Li, *et al.*, Highly Efficient Separation/Recycling Palladium(II) Ions from Aqueous Solutions by Silica Gel-Coated Graphene Oxide Modified with Mercapto Groups, *Metall. Mater. Trans. B*, 2019, **50**, 2747–2757.
73 J. Dobrzyńska, R. Dobrowolski, R. Olchowski, E. Zięba and M. Barczak, Palladium adsorption and preconcentration onto thiol- and amine-functionalized mesoporous silicas with respect to analytical applications, *Microporous Mesoporous Mater.*, 2019, **274**, 127–137.
74 M. I. López, D. Esquivel, C. Jiménez-Sanchidrián, P. Van Der Voort and F. J. Romero-Salguero, Thiol-functionalized ethylene periodic mesoporous organosilica as an efficient scavenger for palladium: Confirming the homogeneous character of the Suzuki reaction, *Materials*, 2020, **13**, 623.
75 B. Leśniewska, *et al.*, Method development for determination of trace amounts of palladium in environmental water samples by ICP-MS/MS after pre-concentration on thiol-functionalized MCM-41 materials, *Talanta*, 2020, **217**, 121004.
76 C. Hinz, Description of sorption data with isotherm equations, *Geoderma*, 2001, **99**, 225–243.
77 G. Limousin, *et al.*, Sorption isotherms: A review on physical bases, modeling and measurement, *Appl. Geochem.*, 2007, **22**, 249–275.
78 M. Barczak, *et al.*, Synthesis and application of thiolated mesoporous silicas for sorption, preconcentration and determination of platinum, *Mater. Chem. Phys.*, 2016, **181**, 126–135.
79 M. Zeizinger, J. V. Burda, J. Šponer, V. Kapsa and J. Leszczynski, A systematic *ab initio* study of the hydration of selected palladium square-planar complexes. A comparison with platinum analogues, *J. Phys. Chem. A*, 2001, **105**, 8086–8092.
80 K. J. Naidoo, G. Klatt, K. R. Koch and D. J. Robinson, Geometric hydration shells for anionic platinum group metal chloro complexes, *Inorg. Chem.*, 2002, **41**, 1845–1849.
81 S. Y. Bratskaya, A. Y. Ustinov, Y. A. Azarova and A. V. Pestov, Thiocarbamoyl chitosan: Synthesis, characterization and sorption of Au(III), Pt(IV), and Pd(II), *Carbohydr. Polym.*, 2011, **85**, 854–861.
82 T. L. Lin and H. L. Lien, Effective and selective recovery of precious metals by thiourea modified magnetic nanoparticles, *Int. J. Mol. Sci.*, 2013, **14**, 9834–9847.
83 E. Vassileva, *et al.*, Solid-phase extraction of heavy metal ions on a high surface area titanium dioxide (anatase), *Analyst*, 1996, **121**, 607–612.
84 M. Kanna, S. Wongnawa and P. Sherdshoopongse, Adsorption behavior of some metal ions on hydrated amorphous titanium dioxide surface, *Songklanakarin J. Sci. Technol.*, 2005, **27**, 1017–1026.
85 C. Huang and B. Hu, Synthesis and characterization of titania hollow fiber and its application to the microextraction of trace metals, *Analyst*, 2011, **136**, 1425.
86 K. Wyns, *et al.*, Iron(III) removal from acidic solutions using mesoporous titania microspheres prepared by vibrational droplet coagulation, *J. Environ. Chem. Eng.*, 2021, **9**, 106257.
87 R. Moordini, A. Badiei and D. Afzali, Separation of trace amounts of palladium from water and wastewater samples using MPTMS-SBA-15 mesoporous silica sorbents, *Sep. Sci. Technol.*, 2017, **52**, 2827–2834.
88 H. Liu, *et al.*, Facile fabrication of CuxSy/Carbon composites using lignosulfonate for efficient palladium recovery under strong acidic conditions, *J. Hazard. Mater.*, 2020, **391**, 122253.
89 L. Zhou, J. Liu and Z. Liu, Adsorption of platinum(IV) and palladium(II) from aqueous solution by thiourea-modified chitosan microspheres, *J. Hazard. Mater.*, 2009, **172**, 439–446.
90 F. B. Biswas, *et al.*, Selective recovery of silver and palladium from acidic waste solutions using dithiocarbamate-functionalized cellulose, *Chem. Eng. J.*, 2021, **407**, 127225.
91 F. Li, *et al.*, Synthesis of Chemically Modified Chitosan with 2,5-Dimercapto-1,3,4-thiodiazole and its Adsorption Abilities for Au(III), Pd(II), and Pt(IV), *J. Appl. Polym. Sci.*, 2009, **113**, 1604–1610.
92 V. N. Losev, *et al.*, Extraction of precious metals from industrial solutions by the pine (Pinus sylvestris) sawdust-based biosorbent modified with thiourea groups, *Hydrometallurgy*, 2018, **176**, 118–128.
93 R. E. C. Torrejos, *et al.*, Multidentate thia-crown ethers as hyper-crosslinked macroporous adsorbent resins for the efficient Pd/Pt recovery and separation from highly acidic spent automotive catalyst leachate, *Chem. Eng. J.*, 2021, **424**, 130379.
94 M. Rajiv Gandhi, M. Yamada, Y. Kondo, A. Shibayama and F. Hamada, F. P-Sulfonatothiacalix[6]arene-impregnated resins for the sorption of platinum group metals and effective separation of palladium from automotive catalyst residue, *J. Ind. Eng. Chem.*, 2015, **30**, 20–28.
95 M. Yamada, S. Kimura, M. Rajiv Gandhi and A. Shibayama, Environmentally friendly Pd(II) recovery from spent automotive catalysts using resins impregnated with a pincer-type extractant, *Sci. Rep.*, 2021, **11**, 1–11.
96 Z. Hubicki, M. Leszczyńska, B. Łodyga and A. Łodyga, Recovery of palladium(II) from chloride and chloride-nitrate solutions using ion-exchange resins with S-donor atoms, *Desalination*, 2007, **207**, 80–86.
97 E. Anticó, A. Masana, V. Salvadó, M. Hidalgo and M. Valiente, Adsorption of palladium by

glycolmethacrylate chelating resins, *Anal. Chim. Acta*, 1994, **296**, 325–332.

98 M. Gurung, *et al.*, Selective recovery of precious metals from acidic leach liquor of circuit boards of spent mobile phones using chemically modified persimmon tannin gel, *Ind. Eng. Chem. Res.*, 2012, **51**, 11901–11913.

99 Y. Kanai, T. Oshima and Y. Baba, Synthesis of highly porous chitosan microspheres anchored with 1,2-ethylenedisulfide moiety for the recovery of precious metal ions, *Ind. Eng. Chem. Res.*, 2008, **47**, 3114–3120.

100 S. Wu, *et al.*, Isopentyl-sulfide-impregnated nano-MnO2 for the selective sorption of Pd(II) from the leaching liquor of ores, *Molecules*, 2017, **22**, 1117.

101 M. Zha, J. Liu, Y. L. Wong and Z. Xu, Extraction of palladium from nuclear waste-like acidic solutions by a metal-organic framework with sulfur and alkene functions, *J. Mater. Chem. A*, 2015, **3**, 3928–3934.

102 S. Phillips, D. Holdsworth, P. Kauppinen and C. Mac Namara, Palladium impurity removal from active pharmaceutical ingredient process streams: A method for scale-up, *Johnson Matthey Technol. Rev.*, 2016, **60**, 277–286.